Raman Dynamic Probe of Hydrogen Exchange in Bean Pod Mottle Virus: Base-specific Retardation of Exchange in Packaged ssRNA

Tiansheng Li,* John E. Johnson,‡ and George J. Thomas, Jr.*

*Division of Cell Biology and Biophysics, School of Biological Sciences, University of Missouri-Kansas City, Kansas City, Missouri 64110 USA

ABSTRACT   We describe a novel approach to investigating exchange kinetics in biological assemblies. The method makes use of a Raman multichannel analyzer coupled with a dialysis flow cell. We employ this methodology to determine exchange rates of labile hydrogens in both the packaged RNA genome and protein subunits of bean pod mottle virus (BPMV). In the BPMV assembly, which is similar to human picornaviruses, the x-ray structure indicates that about 20% of the ssRNA chain is ordered at the threefold vertices of the icosahedral capsid, although the nucleotide bases in the ordered segments are not known (Chen et al., 1989). Here, we compare exchange profiles of the native virus with those of the empty capsid, model nucleic acids and aqueous solvent to reveal the following exchange characteristics of BPMV RNA and protein: (i) Base-specific retardation of exchange is observed in the packaged RNA. (ii) Retardation is greatest for uracil residues, for which the first-order exchange rate constant ($k_U = 0.18 \pm 0.02$ min^{-1}) is 40% lower than that of either the H$_2$O solvent or adenine or cytosine groups of RNA ($k_{solv} \approx k_A \approx k_C = 0.30 \pm 0.02$ min^{-1}). (iii) Retardation of exchange is also observed for the guanine residues of packaged RNA. (iv) No appreciable exchange of amide NH groups of capsid subunits occurs within the time of complete exchange ($t \approx 10$ min) of packaged RNA or bulk solvent. Thus, the present results identify sites in both the protein subunits (amide NH) and RNA nucleotides (amino NH$_2$ and imino NH) which are resistant to solvent-catalyzed hydrogen exchange. We propose that retardation of exchange of labile sites of the RNA nucleotides is a consequence of the organization of the RNA chromosome within the virion. Our findings support a model for BPMV in which surface and buried domains of capsid subunits are extensively and rigidly hydrogen-bonded, and in which uracil and guanine exocyclic donor groups of packaged RNA are the principal targets for subunit interaction at the threefold vertices of the capsid.

INTRODUCTION

The 3.0-Å crystal structure of bean pod mottle virus (Chen et al., 1989), a member of the plant comovirus family, reveals that capsid subunits are arranged on a $P = 3$ lattice and contain the β-barrel fold observed in subunits of picornaviruses and many other icosahedral viruses (Lomonossoff and Johnson, 1991). The bean pod mottle virus (BPMV) *middle* component packages a single-stranded RNA molecule (RNA2) of 2.0×10^6 Da. RNA2 constitutes about 30% of the mass of the middle component particle. The empty capsid, or *top* component, consists of the same subunit assembly as the middle component and is isostructural with it, but lacks the RNA genome. The electron density map of the middle component virion exhibits additional features at the threefold vertices of the capsid, which have been assigned to the packaged single-stranded RNA2 molecule and account for about 20% of its nucleotide residues. The crystal structure shows that the ordered nucleic acid maintains a backbone stereochemistry approximating one strand of A-form RNA and that the nucleotides are in contact with hydrophilic side chains of capsid subunits (Chen et al., 1989). Most of the remaining 80% of nucleotides of the packaged RNA mol-

ecule, though not revealed in the x-ray crystal structure, are shown by Raman spectroscopy to adopt the A-form backbone stereochemistry in the crystal (Li et al., 1990) and to retain this conformation in solutions of the virus (Li et al., 1992). Comparison of the temperature-dependent Raman spectra of BPMV RNA in packaged and unpackaged states shows further that a significant increase in thermostability of RNA secondary structure occurs with packaging. When packaged, BPMV RNA exhibits more phosphodiester groups in the A conformation and enhanced base stacking and base pairing interactions in comparison to unpackaged BPMV RNA (Li et al., 1992). The specific base residues involved in RNA-capsid contacts and further details of their intermolecular association have not been determined.

In order to gain further insight into the organization and interactions of packaged BPMV RNA, we have developed a Raman probe of exchangeable hydrogenic sites of virion constituents. The method is based upon the measurement in real time of the decay of Raman band intensities associated with specific molecular groups of both BPMV RNA and protein, as these groups become progressively exchanged by either deuterium in a D$_2$O-solvent environment, or protium in an H$_2$O-solvent environment (Li, 1992). The Raman dynamic probe described here reports on the solvent accessibility of exchangeable imino (NH) and amino (NH$_2$) sites of specific purine and pyrimidine residues of the packaged single-stranded RNA genome. Simultaneously, the technique reveals solvent accessibility of polypeptide-chain amide (NH) groups of capsid subunits.

Biophysical Journal Volume 65 November 1993

Methods employed previously to investigate labile hydrogen exchange, such as nuclear magnetic resonance spectroscopy and tritium labeling, are either inapplicable to large viral assemblies or unable to resolve exchanges of specific nucleic acid base and protein groups.

At present, little is known about the hydrogen-exchange characteristics of protein and nucleic acid molecules within viruses. The present study focuses on application of the Raman dynamic probe to empty capsids and middle component virions of BPMV. By comparison with exchanges measured on isolated virion components and additional model compounds, we are able to interpret the hydrogen-isotope exchange data from BPMV and discuss the results in relation to existing knowledge of the virus structure. Although hydrogen-isotope exchange has been used extensively in conjunction with spectroscopic methods to probe structures and dynamics of isolated nucleic acids and proteins (see, for example, reviews by Englander and Kallenbach (1984), Englander and Mayne (1992), and Thomas and Tsuboi (1993)), we believe the present application is the first to probe simultaneously the exchangeable sites of nucleic acid and protein molecules in a native virus assembly.

In this investigation we address the following questions: (i) Do solvent molecules penetrate and permeate the interior of the virion and mediate unhindered exchange of labile hydrogenic (NH and NH_2) groups? (ii) Do amide NH groups of the capsid subunits exchange differently in the presence of the packaged RNA molecule? (iii) Do differences exist between the hydrogen-exchange rates of packaged BPMV RNA and protein-free RNA models? (iv) Do the hydrogen-exchange profiles of specific RNA subgroups provide evidence of base-specificity in RNA-protein interactions within the virion?

EXPERIMENTAL PROCEDURES

Isolation and preparation of BPMV components for Raman spectroscopy

The BPMV middle component (virion) and top component (empty capsid) were isolated and purified using established procedures (Semancik and Bancroft, 1965). RNA2 was isolated from the middle component, purified by phenol extraction, and stored as described (MacFarlane et al., 1991). Solutions of virus and capsid were prepared for Raman spectroscopy at approximately 100 $\mu g/\mu l$ in an aqueous buffer, consisting of 0.1 M KCl + 10 mM Tris at pH 7.0. RNA2 solutions were prepared at 50 $\mu g/\mu l$ in the same buffer. Other details of sample preparations for Raman spectroscopy have been given (Li et al., 1992).

Raman flow cell and instrumentation

The Raman flow cell was designed to meet the following requirements. First, the macromolecular concentration within the sample volume exposed to laser Raman excitation, and therefore the corresponding Raman band intensities of the macromolecule, should remain essentially constant under conditions of efflux. Second, the optical homogeneity of the sample solution should not change significantly during efflux, in order to minimize fluctuations in the Raman spectral background. Third, introduction of effluent should not alter more than one solution condition at a time. For example, in studies of hydrogen-isotope exchange, the solution acidity and the concentrations of salts and buffers should remain as nearly constant as possible during exchange.

The flow-cell device consists of a syringe infusion pump (Harvard Apparatus, Model 11) with a custom-designed conical outlet sealed to microdialysis tubing of 200-μm outer diameter and molecular mass cutoff of 6000 Da. The microdialysis tubing is threaded through a conventional glass capillary tube (Kimax #34500) of 1.5-mm inner diameter, which serves as the Raman sample cell and contains the macromolecular solution under investigation. The effluent solution, containing the different isotopic solvent (usually D_2O), is pumped through the dialysis tubing to exchange freely with the surrounding sample solution, in accordance with the tubing pore size and the nature of sample and effluent species. The flow rate of the effluent is precisely controlled by the microinjection pump. Raman spectra are collected as the isotopic exchange progresses. The design of the apparatus and its method of operation in a typical Raman data collection protocol are depicted in Fig. 1. For present studies of BPMV and model compounds, a flow rate of 4.5 ml/h was usually employed. Control experiments showed that flow rates between 2.5 and 60 ml/h give essentially identical results.

Use of this system for monitoring a simple H_2O/D_2O exchange process is exemplified in Fig. 2. In this experiment, 10 μl of D_2O was placed in the sample cell, and H_2O effluent was pumped through the dialysis tubing at the indicated flow rate, while the Raman spectrum in the 700–1700-cm^{-1} interval was collected at 1-min intervals with 10-s data accumulation times. Raman bands at 1204, 1450, and 1640 cm^{-1}, due, respectively, to bending modes of H_2O, HOD, and D_2O species are evident. The protium/deuterium exchange process is time resolved by measurement of either the decrease

RAMAN FLOW CELL
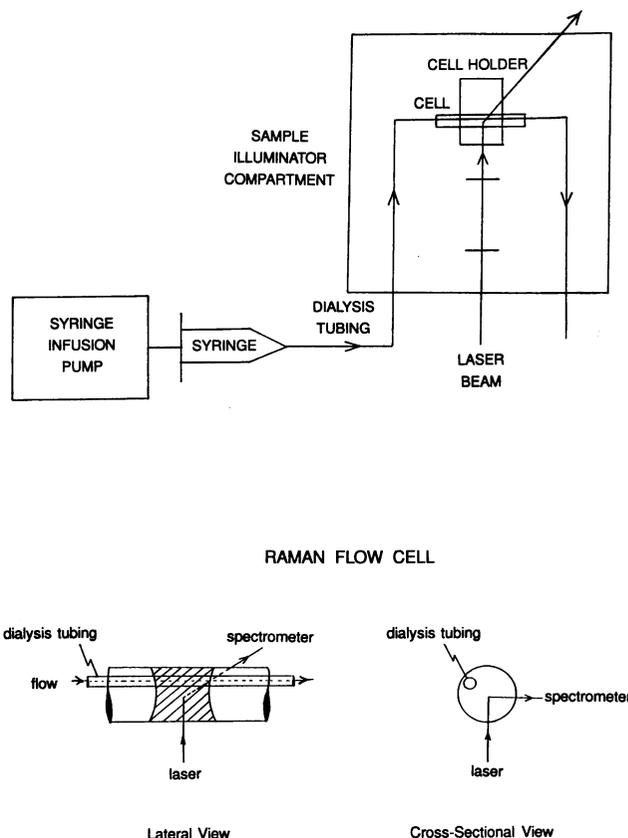

Lateral View   Cross-Sectional View

FIGURE 1 Instrumentation for time-resolved flow-cell Raman spectroscopy. (*Upper*) Block diagram of the apparatus employed for collection of Raman spectra in real time from a solution containing a biological sample subjected to controlled change of the solvent protium/deuterium isotope composition. A similar apparatus has been employed to alter solution acidity or salt composition, while the Raman spectrum is recorded in real time (R. Tuma and G. J. Thomas, Jr., unpublished results). (*Lower*) Lateral and cross-sectional views of the sample cell in the vicinity of the laser focus. The volume of solution employed in the sample cell is approximately 5 μl.
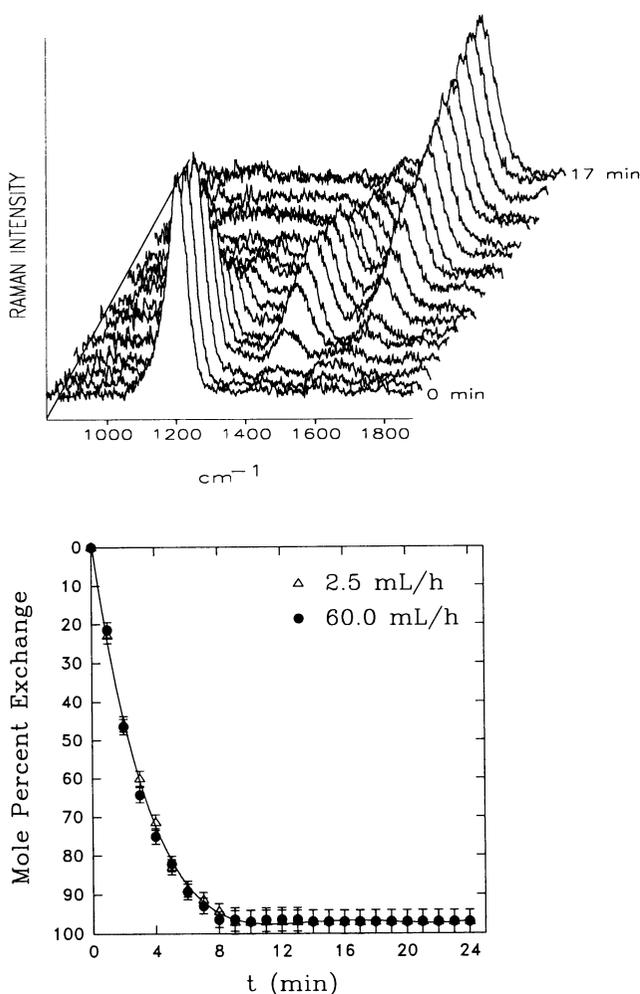
FIGURE 2   *Upper*: A three-dimensional plot showing time evolution of the Raman spectrum of D_2O ($t = 0$) into that of H_2O ($t = 17$ min), using the apparatus described in Fig. 1 with H_2O as the effluent. The D_2O sample volume was 10 μl and the H_2O flow rate through the dialysis tubing was 2.5 ml/h. The Raman intensities (*vertical axis*) are shown for the region 700–1700 cm^{-1} (*horizontal axis*). Each spectrum was obtained with an accumulation time of 10 s. *Lower*: Plot of the mole percent protium exchange of D_2O as measured by the intensity decrease of the 1204 cm^{-1} band (DOD bending mode), with H_2O flow rates of 2.5 ($\triangle$) and 60 ($\bullet$) ml/h. The data fit a single exponential (Eq. 1, *solid line*) with exchange rate constant $k = 0.34 \pm 0.02$ min^{-1}, corresponding to a half-life $t_{1/2} = 2.04 \pm 0.11$ min.

of Raman intensity at 1204 cm^{-1} or increase of Raman intensity at 1640 cm^{-1}, for which the percent exchange, E, can be expressed as

$$E = 100 \, (1 - e^{-kt}), \tag{1}$$

where k is the first-order rate constant. The data of Fig. 2 serve as a control experiment to demonstrate the feasibility of the system and establish an effective "time constant" for exchange of bulk solvent (in this case, D_2O) when its isotopic complement (H_2O) is employed as the effluent. The data fit Eq. 1 with $k = 0.34 \pm 0.02$ min^{-1} = 0.0057 ± 0.0003 s^{-1}. This represents an upper limit (i.e., fastest exchange rate) which can be measured with the present system. Exchange processes with significantly shorter half-lives ($t_{1/2} < 2$ min) will not be time resolved.

In a typical experimental protocol on a nucleic acid or protein solution, the 700–1700 cm^{-1} region of the spectrum will also contain bands due to the dissolved macromolecule. In principle, either the 1204 (D_2O) or 1640 (H_2O) cm^{-1} band could be used to compare the exchange profile of the solute with that of solvent. Such an approach requires that overlap between bands

of solute and solvent can be appropriately compensated. This is often, but not always, the case. When the solute band of interest overlaps either solvent band (bending mode noted above), the solute band in question is more conveniently compared with the O-H "stretching" band which extends from 3000–3700 cm^{-1}. The latter is well removed from solute markers of interest and its intrinsically high intensity facilitates accurate intensity measurements. Despite the complex origins of the 3000–3700 cm^{-1} band, its normalized integrated intensity (I_{OH}/I_{CH}) is essentially linearly dependent upon the total fraction of solvent O—H oscillators in solution (f_{OH}) over a wide range of protium concentration (0–90%). This linear relationship, with the desirable zero intercept, is shown for a control experiment on solutions of polyethyleneglycol (PEG-8000) in Fig. 3 and Table 1.

Further details of the flow-cell assembly and its H_2O/D_2O exchange characteristics have been described (Li, 1992). A Raman flow cell for measurement of cation-induced structural changes in perfused muscle fibers has also been described by Pézolet and co-workers (Caillé et al., 1983). The novel aspect of the present design is its suitability for time resolution of kinetic processes in macromolecular assemblies.

For the collection of Raman spectra, the flow-cell assembly was placed in the sample illuminator compartment of a Raman triple spectrograph (Model 1877; Spex Triplemate, Metuchen, NJ) equipped with an optical multichannel analyzer (OMA-III, EG&G, Princeton, NJ) and intensified 1024-diode array detector (Lamba et al., 1990). Raman spectra were excited with the 514.5-nm line of an argon laser (Coherent Innova 70, Santa Clara, CA), using approximately 100 mW of radiant power at the sample. Further details of the spectrometer are described elsewhere (Lamba et al., 1990). Typically, two different spectral band passes were employed to span the spectral regions 640–1750 and 2750–3750 cm^{-1}. Multiple spectra were captured with exposure times between 10 and 20 s, and the spectral signals were averaged to improve signal-to-noise ratios.

Processing of spectral data was performed with Sigma Plot and SpectraCalc software on an IBM microcomputer. In the computation of Raman difference spectra between different periods of hydrogen-isotope exchange of RNA, we employed the 1100 cm^{-1} Raman band of the phosphodioxy group as the internal intensity standard. This band is unaffected by base deuterations (Lafleur et al., 1972; Prescott et al., 1974) and is well resolved from other spectral features. For protein difference spectral computations, the 1003 cm^{-1} band of the phenylalanyl group, which is not deuteration sensitive (Li et al., 1992), was employed as the internal intensity standard. Additional experimental procedures relating to Raman spectroscopy of BPMV and Raman difference computations on BPMV components have been further discussed by Li et al. (1992).

All exchange experiments described in the following sections were repeated at least in triplicate, and in each separate protocol yielded identical results within the indicated experimental uncertainties. In each case, the quoted limit of error is determined by the repeatability of the result among separate protocols and the noise level (uncertainty) in the experimentally measured spectral intensity.

RESULTS AND DISCUSSION

Hydrogen exchange characteristics of proteins and nucleic acids

Solvent exchange of amide NH groups is catalyzed by acids and bases, particularly H_3O^+ and OH$^-$. Such exchanges in proteins and polypeptides have been investigated extensively, and reviews have been given recently (Englander and Kallenbach, 1984; Englander and Mayne, 1992). In a random-chain polypeptide, such as poly-D,L-alanine at pH 7 and 20°C, the experimentally observed average rate is approximately 57 s^{-1}, corresponding to a half-life $t_{1/2}$ of 12 ms (Jeng and Englander, 1991). For globular proteins, however, amide exchange rates are often orders of magnitude slower than those of random-chain polypeptides and oligopeptides. Retardation of NH exchange in proteins is a result of the
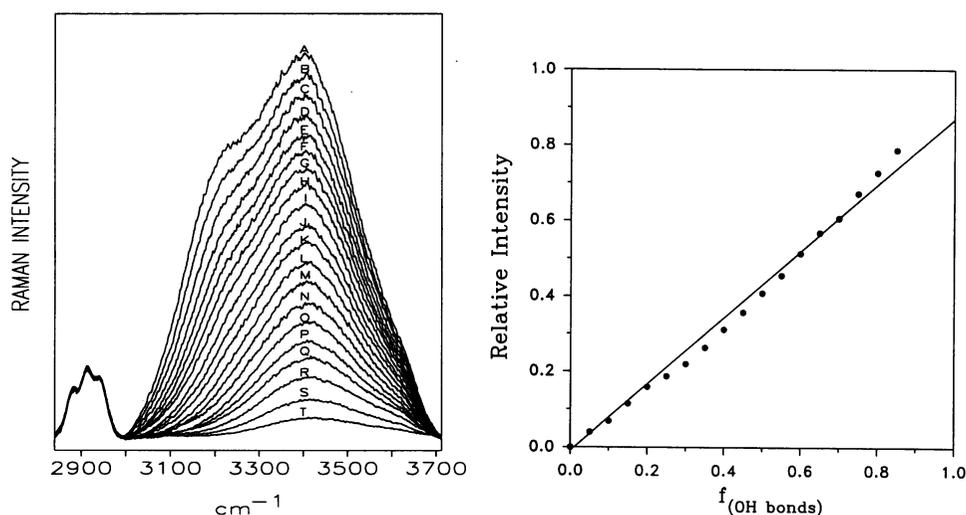
FIGURE 3   *Left*: Raman spectra in the region 2840–3710 cm^{-1} of a series of H_2O + D_2O mixtures (25°C, pH 7) containing the initial percent composition of H_2O (%H_2O) and equilibrium percent compositions of H_2O, D_2O, and HOD indicated in Table 1. The water band extends from 3000 to 3700 cm^{-1}. The triplet of bands below 3000 cm^{-1} is due to polyethyleneglycol solute (PEG-8000, 5wt%), employed in this control experiment as an internal intensity standard. *Right*: Plot of the integrated and normalized intensity of the 3000–3700 cm^{-1} water band (I_{OH}/I_{CH}) versus the fraction of O—H oscillators in solution (f_{OH} = initial H_2O concentration), for the data shown at left. The linear curve with zero intercept exhibits slope = 0.88 and correlation coefficient = 0.99.

three-dimensional structure, and has been attributed specifically to involvement of the NH donor in hydrogen bonding interaction (Englander and Kallenbach, 1984). Accordingly, NH exchanges in proteins require transient separation of peptide group hydrogen bonds and, therefore, are strongly influenced by temperature, pH, interactions with the aqueous solvent, and quaternary protein structure. Since a large fraction of the amide NH groups in a globular protein the size of the average BPMV subunit (molecular mass of 24 kDa) is expected to exist at or near the protein surface, the average NH exchange rate in BPMV should be highly dependent upon the assembly state.

In nucleic acids, as in proteins, hydrogen exchange requires hydrogen-bond separation. This has been demonstrated for amino (NH_2) and imino (NH) protons in base-paired nucleotides of Watson-Crick duplexes and is evidently due to the transient separation of base pairs in the double helix (Teitelbaum and Englander, 1975; Mandal et al., 1979). In (rA)·(rU) and (rI)·(rC) duplexes, the base-pair opening rate, which limits the rate of NH/NH_2 hydrogen exchanges, falls within the range 1–100 s^{-1} at pH 6 and 20°C.

Hydrogen exchange profiles of polyribonucleotides

In order to investigate exchange rates of labile protons of RNA nucleotides in the absence of protein, we monitored the shift of deuterium-exchange-sensitive Raman bands of protein-free model RNAs (synthetic polyribonucleotides) using the experimental system described in Fig. 1. Parallel studies were also carried out on unpackaged BPMV RNA and on ribosomal RNA isolated from *Escherichia coli*, both of which exhibited no apparent differences from the synthetic RNA models. The superior resolution and signal-to-noise ratios obtained from spectra of the RNA models permitted the most accurate determinations of the base-specific exchange rate constants, which are compared below with those obtained from BPMV. The results and interpretations are next discussed.

Poly(rU)

The uracil residue exhibits a number of intense Raman bands in the spectral region 300–1800 cm^{-1} (Lord and Thomas,

TABLE 1   Equilibrium compositions of H_2O, D_2O, and HOD in solutions described in Fig. 3

Solution (%H_2O)	$[H_2O]_{eq}$	$[D_2O]_{eq}$	$[HOD]_{eq}$	Solution (%H_2O)	$[H_2O]_{eq}$	$[D_2O]_{eq}$	$[HOD]_{eq}$
A (100)	100	0	0	K (50)	25	25	50
B (95)	90.25	0.25	9.5	L (45)	20.25	30.25	49.5
C (90)	81.0	1.0	18.0	M (40)	16.0	36.0	48.0
D (85)	72.25	2.25	25.5	N (35)	12.25	42.25	45.5
E (80)	64.0	4.0	32.0	O (30)	9.0	49.0	42.0
F (75)	56.25	6.25	37.5	P (25)	6.25	56.25	37.5
G (70)	49.9	9.0	42.0	Q (20)	4.0	64.0	32.0
H (65)	42.25	12.25	45.5	R (15)	2.25	72.25	25.5
I (60)	36.0	16.0	48.0	S (10)	1.0	81.0	18.0
J (55)	30.25	20.25	49.5	T (5)	0.25	90.25	9.5

1967). Deuteration of the ring imino (3NH) group causes substantial changes in several of these bands (Lafleur et al., 1972; Prescott et al., 1974), particularly those in the spectral intervals 1200–1300 and 1600–1700 cm^{-1}. Fig. 4 shows time-resolved changes in the spectral region 700–1700 cm^{-1} as uracil 3NH groups of poly(rU) are deuterated, as well as
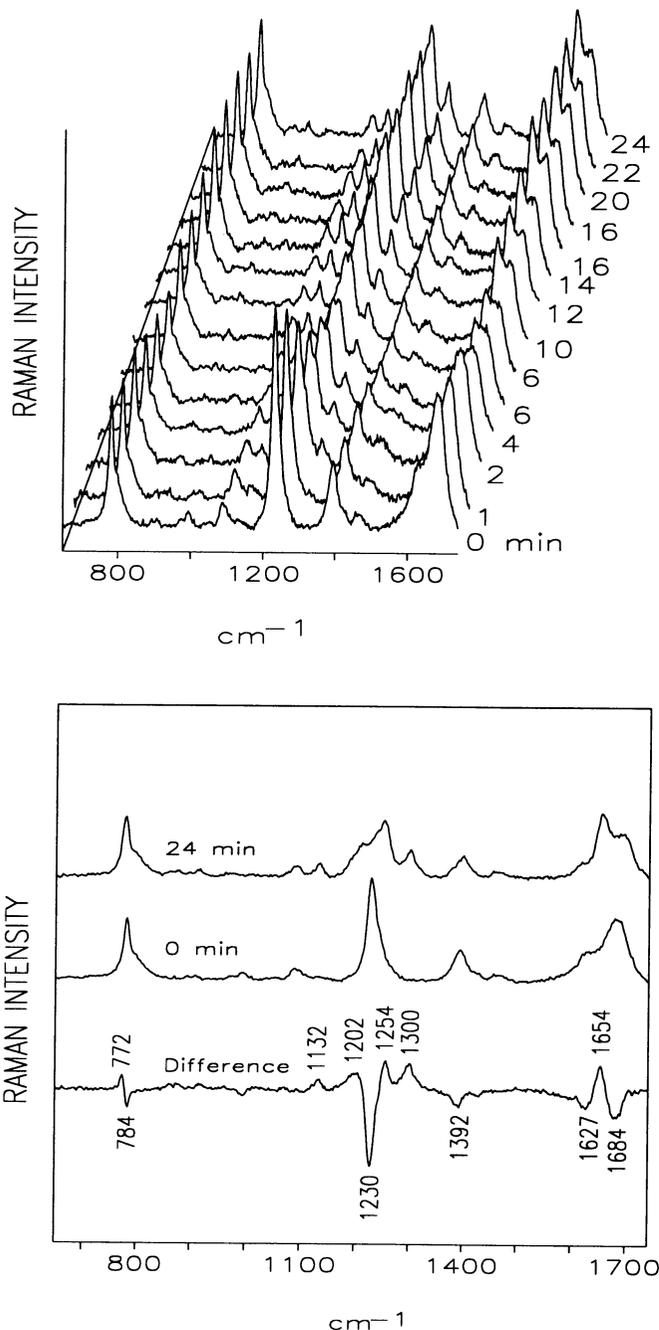
the difference spectrum computed between 3ND and 3NH forms of poly(rU). Difference bands are observed at 772, 784, 1132, 1202 (D$_2$O), 1230, 1254, 1300, 1392, 1627, 1654, and 1684 cm^{-1}. The intensity decay at 1230 cm^{-1}, which is the most intense feature distinguishing nondeuterated and deuterated uracil rings, is the most favorable for calculating the kinetics of deuterium exchange of 3NH groups in poly(rU).

In order to compare and relate the kinetics of deuteration of poly(rU) with the change in hydrogen/deuterium (H/D) composition of the solvent during efflux, it is necessary to measure simultaneously the intensity decay of an isotope-sensitive Raman band of the solvent. For this purpose we have employed the integrated intensity of the solvent O—H stretching band (3000–3700 cm^{-1}), which, as noted above (Fig. 3), is an indicator of the total protium concentration in solution (f_{OH}). Normalized intensity decays of the uracil (1230 cm^{-1}) and solvent markers (3000–3700 cm^{-1}) are compared in Fig. 5. The observed first order decay rates (Eq. 1) for poly(rU) ($k_U = 0.29 \pm 0.02$ min^{-1}) and solvent ($k_{solv} = 0.30 \pm 0.02$ min^{-1}) are indistinguishable kinetically and within experimental uncertainty of the value observed for pure solvent (cf. Fig. 4). Thus, the rate of uracil 3NH exchange in poly(rU) is determined by the time constant of the presently employed experimental system. The same results are obtained on poly(rA)·poly(rU) (data not shown). Exchange measurements by stopped-flow UV spectroscopy on poly(rA)·poly(rU) at 20°C and pH 6 indicate exchange rates for both uracil 3NH (66 min^{-1}) and adenine 6NH$_2$

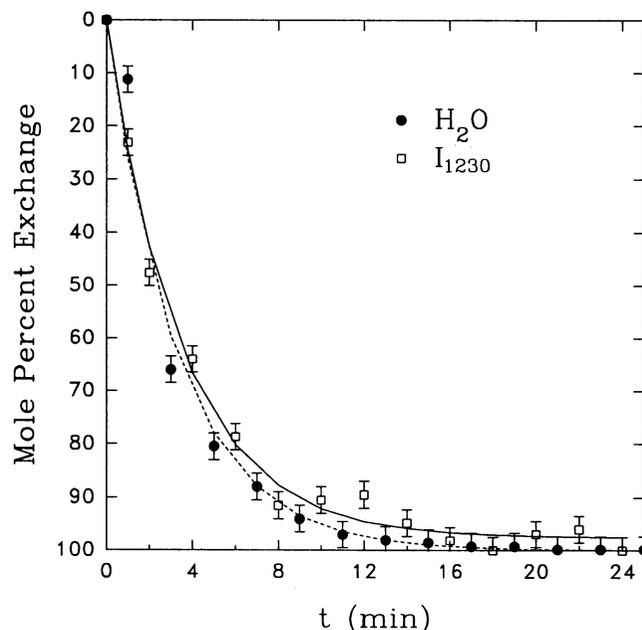FIGURE 4 *Upper*: Time-resolved changes in the Raman spectrum of poly(rU) accompanying deuteration of uracil 3NH groups, as revealed by spectra collected at 2-min intervals between 0 and 24 min using the apparatus of Fig. 1. The accumulation time for each spectrum was 20 s. Data were obtained from H$_2$O solutions of poly(rU) at 50 mg/ml in 0.1 M KCl + 10 mM Tris (pH 7) and 25°C, with corresponding D$_2$O buffer effluent at 4.5 ml/h. *Lower*: Raman difference spectrum (*bottom*) computed between 3ND (*top*) and 3NH (*middle*) forms of poly(rU).

FIGURE 5 Plots of the mol% deuterium exchange of 3NH groups of poly(rU) (□) and OH groups of solvent (●) versus time of D$_2$O efflux for the experiment of Fig. 4. The uracil (3NH isotope) and solvent (OH) concentrations were determined from intensities of the Raman bands at 1230 and 3000–3700 cm^{-1}, respectively. Least-squares fitting of data points to a single exponential (Eq. 1) yields $k_U = 0.29 \pm 0.02$ for poly(rU) and $k_{solv} = 0.30 \pm 0.02$ min^{-1} for solvent.

groups (1.8×10^4 min^{-1}) which significantly exceed the upper limit of detection of the present experimental system (Mandal et al., 1979).

Poly(rC)

Exchange of the exocyclic amino group (4NH$_2$) of cytosine generates significant changes in the Raman spectrum of poly-(rC) and its complexes (Lord and Thomas, 1967; Prescott et al., 1974; Chou and Thomas, 1977). Fig. 6 (*upper*) compares Raman spectra in the 650–1700 cm^{-1} region of 4NH$_2$ and 4ND$_2$ forms of poly(rC). Difference bands are observed at 773, 784, 1178, 1202 (D$_2$O), 1244, 1302, 1504, 1526, and 1600 cm^{-1}. The band at 784 cm^{-1} is the most effective for monitoring the 4NH$_2 \rightarrow$ 4ND$_2$ exchange reaction. Time-resolved data, analogous to that shown for poly(rU) in Figs. 4 and 5 yield the decay curves included in Fig. 6 (*upper*). The results ($k_C = k_{solv} = 0.29 \pm 0.03$ min^{-1}) again indicate that the observed nucleotide exchange rate is limited only by the time constant of the system.

Poly(rG)·poly(rC)

Both poly(rG) and guanine mononucleotides are capable of various associative interactions which greatly complicate

their Raman spectra (Rice et al., 1973). Accordingly, we employed the poly(rG)·poly(rC) duplex to model exchange of guanine nucleotide imino (1NH) and exocyclic amino (2NH$_2$) groups, and also to permit comparison of cytidylyl 4NH$_2$ exchange in the duplex with that observed in single-stranded poly(rC). The results are shown in Fig. 6 (*lower*). The spectrum of deuterated poly(rG)·poly(rC) is similar to that published previously (Lafleur et al., 1972), and the difference spectrum between deuterio and protio forms exhibits bands assignable to cytidylyl (C) and guanylyl (G) residues as follows: 773 (C), 785 (C), 1202 (D$_2$O), 1256 (C), 1303 (C, G), 1470 (G), 1485 (G), 1500 (C), 1582 (G), 1606 (C, G), and 1700 (G, C) cm^{-1}. The bands at 785 (C) and 1485 (G) cm^{-1} are the most sensitive, respectively, to exchange of cytosine 4NH$_2$ and guanine 1NH plus 2NH$_2$ groups. Their intensity decay profiles are included in Fig. 6 (*lower*). Least-squares fits of these experimental data with Eq. 1 give $k_C = 0.28 \pm 0.02$ min^{-1}, $k_G = 0.27 \pm 0.02$ min^{-1} and $k_{solv} = 0.30 \pm 0.03$ min^{-1}. The results indicate again that the exchange rates are limited by the time constant of the system. This is consistent with the more rapid exchanges which have been measured by stop-flow UV spectroscopy on similar model structures (Nakanishi et al., 1977; Preisler et al., 1981). We observe no significant difference between the cytosine exchange rates in single-stranded poly(rC) and double-stranded poly(rG)·poly(rC).

Poly(rA)

In comparison to the deuteration effects noted above for U, C, and G residues, deuteration of the adenine exocyclic 6NH$_2$ group produces smaller changes in the Raman spectra of adenylate derivatives (Lord and Thomas, 1967; Prescott et al., 1974). Scant data (not shown) on poly(rA) and poly-(rA)·poly(rU) indicate an adenine 6NH$_2$ exchange rate consistent with those reported above for other polyribonucleotide models.

Hydrogen exchanges of BPMV

Top component

Deuteration of the peptide NH group leads to well characterized changes in the Raman spectra of proteins. The extensive literature on this subject has been reviewed recently by Bandekar (1992). The most dramatic spectral change accompanying amide NH deuteration is the shift of intense conformation markers in the 1240–1300 cm^{-1} interval (amide III modes) to the 930–990 cm^{-1} interval (amide III'). Peptide NH $\rightarrow$ ND exchange is thus clearly evident in the Raman spectrum of a protein and virtually no solvent interference is encountered.

Time-resolved Raman spectra of the empty BPMV capsid (top component) were collected in the 840–1720 cm^{-1} interval to investigate the kinetics of peptide group exchanges in subunits of the RNA-free capsid. Spectra obtained from an H$_2$O solution buffer of the top component, both before and after extensive D$_2$O buffer efflux, are compared in Fig. 7 (*left*). The difference spectrum of Fig. 7, particularly the
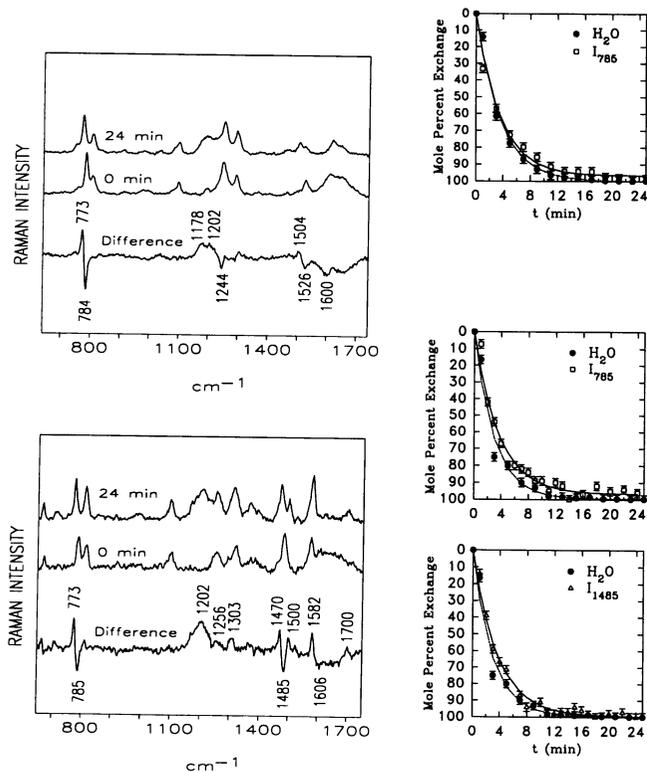

FIGURE 6 Raman spectra of model nucleotide systems in deuterio and protio forms (left panels), and corresponding Raman band intensity decay profiles for solute and solvent species (*right panels*). Time-resolved spectra were obtained for each solution at conditions analogous to those given for poly(rU) in Fig. 4. Data points, labels and fitted curves are similar to those described in the caption of Fig. 5. *Upper*: Poly(rC): $k_C = 0.29 \pm 0.03$ min^{-1}, $k_{solv} = 0.29 \pm 0.02$ min^{-1}. *Lower*: Poly(rG)·poly(rC): $k_C = 0.28 \pm 0.02$ min^{-1}, $k_G = 0.27 \pm 0.02$ min^{-1}, and $k_{solv} = 0.30 \pm 0.03$ min^{-1}.
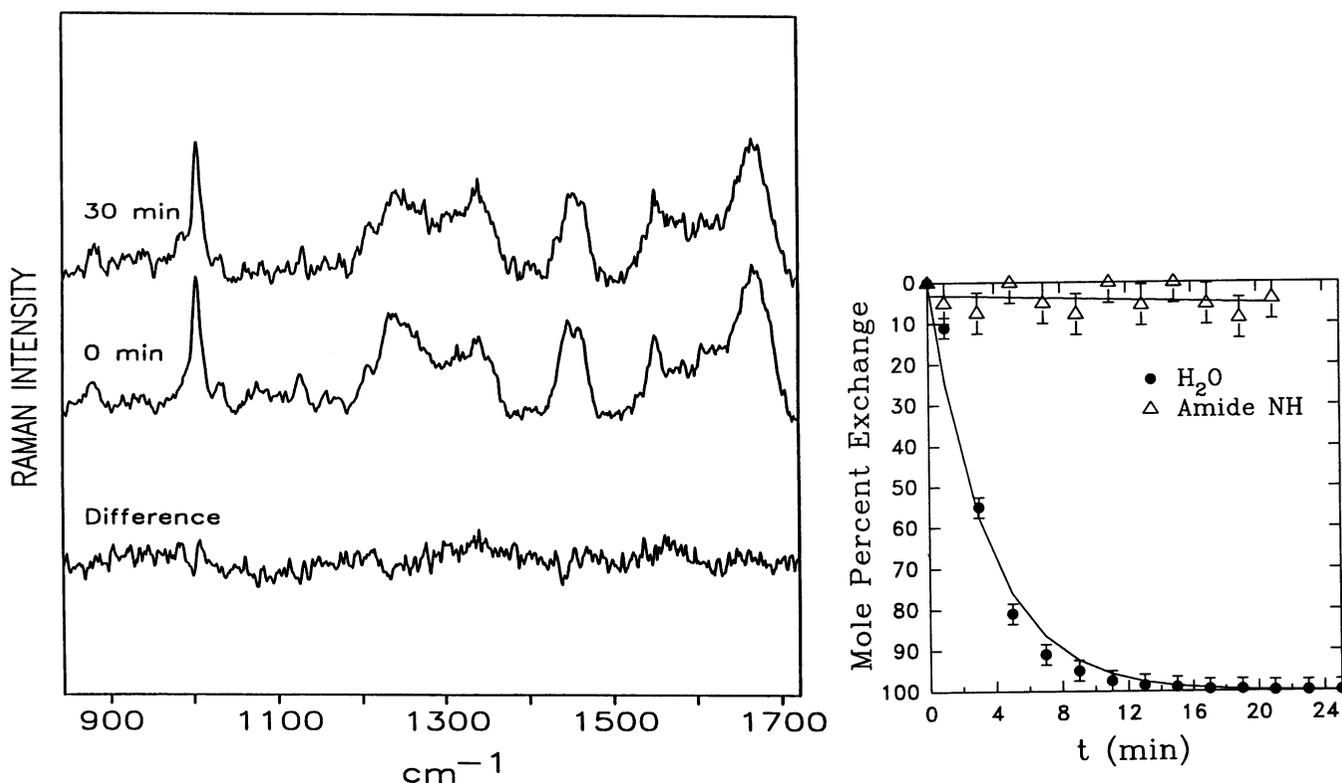
FIGURE 7 *Left*: Raman spectra in the region 850–1720 cm^{-1} of the BPMV top component at exchange times $t = 0$ (*middle*) and $t = 30$ min (*top*), and their difference spectrum (*bottom*). The top component was dissolved to approximately 100 μg/μl in 0.1 M KCl + 10 mM Tris (pH 7.0) and data were collected at 25°C. Initially, 10 μl of the top component solution was placed in the Raman cell and the corresponding D$_2$O buffer was pumped through the dialysis tubing at 4.5 ml/h while Raman spectra were collected. *Right*: Plots of Raman amide III intensity ($\triangle$) and of the mol% deuterium exchange of solvent in the BPMV top component solution as measured by the intensity decrease of the solvent O—H band at 3000–3700 cm^{-1} ($\bullet$). The f_{OH} data fit a single exponential (Eq. 1) with exchange rate constant $k_{solv} = 0.30 \pm 0.02$ min^{-1}.

amide III and amide III' regions, shows no evidence of difference bands beyond the intrinsic noise level of the data ($\pm 8\%$). Accordingly, significant NH → ND exchange does not occur in the BPMV top component. Concurrent time-resolved measurements of the solvent O—H band (3000–3700 cm^{-1}), with appropriate normalization to the C—H stretching band (2800–3000 cm^{-1}) of the top component, confirm that $k_{solv} = 0.30 \pm 0.02$ min^{-1} in this experiment (Fig. 7, *right*). These results demonstrate that at most a small fraction (<10%) of peptide NH groups of BPMV capsid subunits is exchangeable at the same conditions which permit complete exchange of solvent.

Middle component

Time-resolved Raman spectra of the BPMV middle component in H$_2$O buffer during the first 10 min of D$_2$O efflux are shown in Fig. 8. The numerous bands in the Raman spectrum of the virus, for both H$_2$O and D$_2$O solutions, have been reported, and their assignments and structural significance have been discussed in detail previously (Li et al., 1992). The middle component spectrum obtained after 24 min of D$_2$O efflux, and its computed differences from the original spectrum, are redrawn in Fig. 9 (*upper*). All difference bands, namely, at 712 (A), 726 (A), 772 (C), 784 (C), 1162 (U), 1230 (U), 1250–1300 (U), 1348 (A, G), 1469 (G, A), 1484 (G, A),

1562 (G, A), and 1580 (G, A) cm^{-1}, are due exclusively to the packaged RNA2 molecule. In particular, it should be noted that there is no positive difference band near 900–1000 cm^{-1} (amide III' region) in the difference spectrum of Fig. 9 that could be attributed to peptide NH deuteration. Therefore, the negative difference band at 1230 cm^{-1} is attributable entirely to uracil 3NH deuteration. Accordingly, NH and NH$_2$ groups of adenine (726 → 712 cm^{-1}), cytosine (784 → 772 cm^{-1}), guanine (1484 → 1469 cm^{-1}), and uracil (1230 → 1250–1300 cm^{-1}) residues of the packaged RNA are substantially exchanged, while peptide NH groups of virion subunits are essentially resistant to exchange in this experiment.

Also shown in Fig. 9 (*lower*) are the decays of Raman intensities corresponding specifically to deuterium exchanges of cytosine and uracil residues of packaged RNA2 in the middle component virion. Each pyrimidine exchange profile is compared with that of its solvent. The data reveal that cytosines of packaged RNA2 exchange their 4NH$_2$ groups ($k_C^{RNA} = 0.32 \pm 0.04$ min^{-1}) as rapidly as those of solvent and those of either poly(rC) or poly(rC)·poly(rG). This fact alone indicates that solvent access to the packaged genome is as rapid as the time constant of the system permits. However, uracils of packaged RNA2 exhibit significant retardation of 3NH exchange ($k_U^{RNA} = 0.18 \pm 0.02$ min^{-1}) in comparison to solvent or poly(rU) or poly(rA)·poly(rU).
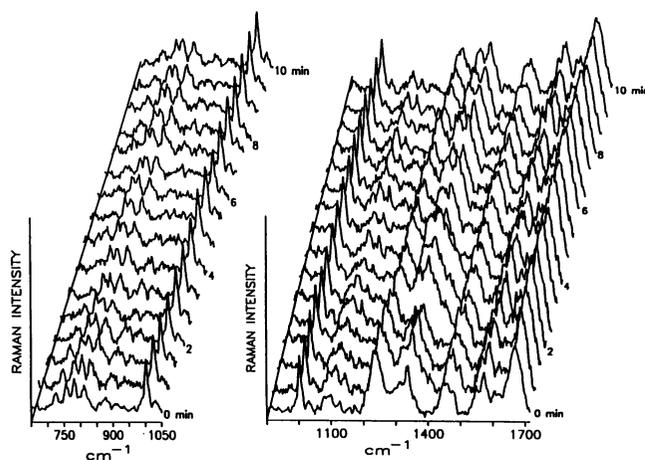
FIGURE 8   Time-resolved Raman spectra in the intervals 650–1050 (*left*) and 900–1700 cm^{-1} (*right*) of the BPMV middle component between 0 and 10 min at 40-s intervals. The middle component was dissolved to approximately 100 μg/μl in 0.1 M KCl + 10 mM Tris (pH 7.0) and data were collected at 25°C. Initially, 10 μl of the middle component solution was placed in the Raman cell and the corresponding D$_2$O buffer was pumped through the dialysis tubing at 4.5 ml/h, while Raman spectra were collected. Data shown are 10-s exposures. The experiment was repeated three times and the corresponding Raman spectra at identical time points were averaged.

The same large and specific retardation of uracil exchange in packaged BPMV RNA was observed in three separate experimental protocols. As noted above, the intrinsic exchange rate of uracil in poly(rA)·poly(rU) is much more rapid than that observed here. Clearly, base pairing involving the uracil 3NH group cannot account for the retardation observed in packaged RNA2. A more likely explanation is that specific RNA-protein interactions between packaged RNA2 and capsid subunits of BPMV retard the uracil 3NH exchanges.

The difference spectra of Fig. 9 (*upper*) also reveal that adenines of RNA2 exchange without measurable retardation vis-a-vis the model systems discussed earlier. This is evidenced by the shift of the adenine band at 726 cm^{-1} (*trough*) to 712 cm^{-1} (*peak*). However, the bands in the interval 1450–1600 cm^{-1} of Fig. 9, which are diagnostic principally of guanine exchange, are much less perturbed in packaged RNA than in model compounds (cf. Fig. 6). This indicates substantial hindrance to guanine 1NH + 2NH$_2$ exchanges in packaged RNA. Due to band overlap in this spectral region, direct measurement of the guanine exchange rate is not feasible.

CONCLUSIONS

We have described a sample flow cell for use in conjunction with Raman optical multichannel spectroscopy to time-resolve hydrogen-isotope exchange reactions of protein and RNA components in viruses. The system requires only microliter volumes of the initial substrate and perturbing effluent solutions. Either H$_2$O or D$_2$O may be employed as the effluent solvent. Hydrogen-exchange processes with half lives of the order of a few minutes can be resolved using this
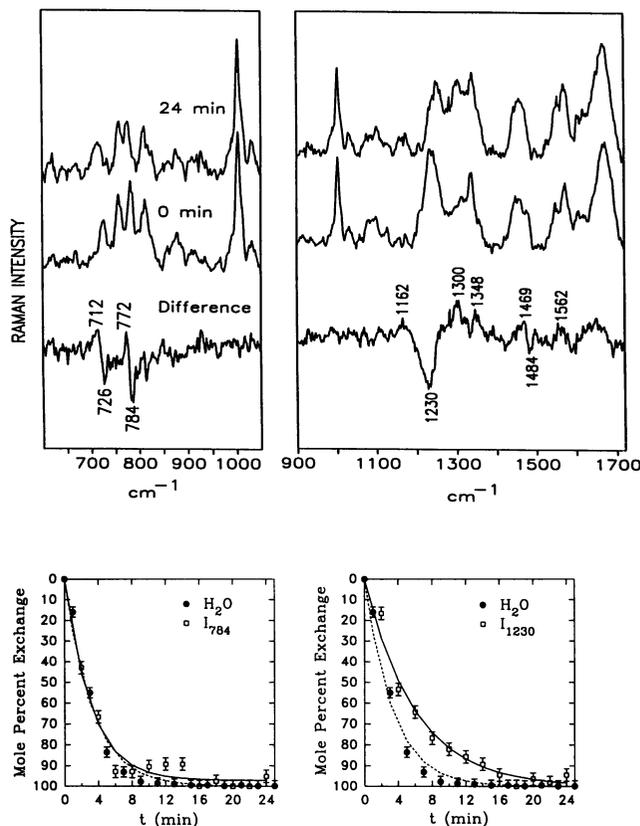

FIGURE 9   *Upper*: Raman spectra in the regions 600–1050 (*left*) and 900–1700 cm^{-1} (*right*) of the BPMV middle component at exchange times $t = 0$ (*middle*) and $t = 24$ min (*top*), and their difference spectrum (*bottom*), corresponding to the experiment of Fig. 8. Other conditions are given in Fig. 8. *Lower*: Plots of the mol% deuterium exchange of cytosine 4NH$_2$ groups (*left*) and uracil 3NH groups (*right*) of packaged BPMV RNA, each compared with solvent OH exchange in the same solution. Data are from the experiment of Fig. 8 and labels and fitted curves are as described in Fig. 5. Least-squares fitting of data points to single exponentials (Eq. 1) yields the following rate constants: $k_C^{RNA} = 0.32 \pm 0.02$ for cytosine of packaged RNA, $k_U^{RNA} = 0.18 \pm 0.02$ for uracil of packaged RNA, and $k_{solv} = 0.32 \pm 0.02$ min^{-1}.

system. The methodology has been applied here to the middle component of bean pod mottle virus.

The present results show that hydrogen exchange of subunit amide groups in the BPMV middle component (virion) does not occur to an appreciable extent, despite unhindered exchange of specific subgroups of the RNA2 molecule packaged within. Similarly, the subunits of the BPMV top component (empty capsid) are resistant to amide exchange at the same conditions which permit the free flow of aqueous solvent through the empty capsid. We interpret these results as evidence that the vast majority (>90%) of amide NH groups of the BPMV capsid are engaged in relatively rigid hydrogen-bonding interactions, since such interactions are considered rate-determining of amide NH exchanges in globular proteins (Englander and Kallenbach, 1984). Because the exchange characteristics of the BPMV subunit are essentially independent of RNA packaging, we conclude further that the resistance of amide groups to solvent-catalyzed hydrogen exchange is the combined result of the secondary,

tertiary, and quaternary protein structures which define the assembled capsid. The subunit secondary structure alone (Chen et al., 1989) is not sufficient to account for more than an estimated 50% of the restricted hydrogen exchange of BPMV subunits.

We have also determined that substantial *base-specific* retardation of exchange occurs for packaged RNA of the BPMV middle component. The rate of uracil (3NH) exchange is 40% slower than that of cytosine ($4NH_2$); and differences are also apparent in the rates of guanine ($1NH + 2NH_2$) and adenine ($6NH_2$) exchanges of packaged RNA, with the former retarded in comparison to the latter. This is the first evidence that packaging of RNA in a viral capsid significantly retards hydrogen-isotope exchange of labile RNA subgroups. We attribute the retardation of exchange of uracil (and probably of guanine) groups of RNA2 to specific RNA-subunit interactions. Such an interpretation is consistent with evidence from equilibrium Raman studies of BPMV (Li et al., 1990; Li et al., 1992), which show that packaging of RNA2 stabilizes, significantly and specifically, interactions involving the uracil residues. The consistency between the present findings and the detection of icosahedrally ordered domains of RNA in the virus crystal structure (Chen et al., 1989) further supports the previous evidence (Li et al., 1990) that the RNA-protein interactions in the crystal structure are retained in the solution structure of BPMV.

Our results suggest that labile hydrogenic sites of uracil (3NH), and possibly also of guanine (1NH and/or $2NH_2$), may be the principal targets of protein side-chain recognition in the BPMV ribonucleoprotein assembly. A structural feature shared by uracil and guanine, but not by cytosine and adenine, is the location of three contiguous hydrogen-bonding sites along a single edge of the heterocycle. We speculate that the 4CO-3NH-2CO network of uracil and $6CO-1NH-2CNH_2$ network of guanine may serve more diverse roles in amino acid side-chain recognition than the corresponding donor and acceptor groups of adenine and cytosine, thus facilitating more extensive and presumably more rigid contacts with capsid subunits. In such a model, the RNA domains which interact with protein side chains are expected to be largely unpaired, i.e., relatively deficient in helical hairpins, and intrinsically flexible, thereby facilitating the formation of thermodynamically stable RNA-protein structures. The prevalence of uracil residues in such regions of RNA2 is consistent with both the primary structure of RNA2 (31% U) and the expectation that uracil-rich single-stranded regions of RNA should be poorly stacked and relatively easily accomodated into clefts of the subunit surface.

MacFarlane et al. (1991) performed computer-aided analysis of the nucleotide sequence of RNA2 in search of reiterated sequences which might explain why ordered RNA is visible in the electron-density map of the middle component. They observed "over-represented" pentameric clusters and a consensus sequence which was repeated 15 times within the RNA2 sequence. Interestingly, these sequential repeats are richest in uracil.

The present study provides the first direct experimental evidence that interchange of the aqueous solvent with the interior cavity of an icosahedral RNA virus is complete within minutes, that the surface and buried domains of the capsid subunits are resistant to solvent-catalyzed exchange, and that there is substantial retardation of exchange of labile sites of the packaged genome. Future studies will focus on reducing the time constant of the system to better characterize the rate of solvent penetration of the virus interior, and on comparing results for different virus assemblies in order to determine whether the same types of base residues suffer retardation of exchange of labile sites.

The methodology developed here has considerable potential for probing other assembly and disassembly processes of viruses. For example, it should be feasible to monitor in real time the pH-induced swelling of an RNA bromovirus, such as cow pea chlorotic mottle virus (CCMV), by appropriate changes of the buffer medium using the present Raman flow system. Similar applications can be envisioned for other biological assemblies. In future developments of the instrumentation employed in this work, we propose to implement charge-coupled-device (CCD) detection of the Raman signals to enable substantially improved measurement of Raman intensity decays. This should facilitate quantitative determination of decay rates for all base residues of packaged viral genomes.

REFERENCES

Bandekar, J. 1992. Amide modes and protein conformation. *Biochim. Biophys. Acta.* 1120:123–143.

Caillé, J.-P., M. Pigeon-Gosselin, and M. Pézolet. 1983. Laser Raman study of internally perfused muscle fibers. Effect of Mg^{2+}, ATP, and Ca^{2+}. *Biochim. Biophys. Acta.* 758:121–127.

Chen, Z., C. V. Stauffacher, Y. Li, T. Schmidt, W. Bomu, G. Kamer, M. Shanks, G. Lomonossoff, and J. E. Johnson. 1989. Protein-RNA interactions in an icosahedral virus at 3.0 Å resolution. *Science (Wash.).* 245: 154–159.

Chou, C. H., and G. J. Thomas, Jr. 1977. Raman spectral studies of nucleic acids XVI. Structures of polyribocytidylic acid in aqueous solution. *Biopolymers.* 16:765–789.

Englander, S. W., and N. R. Kallenbach. 1984. Hydrogen exchange and structural dynamics of proteins and nucleic acids. *Q. Rev. Biophys.* 4: 521–655.

Englander, S. W., and L. Mayne. 1992. Protein folding studied using hydrogen-exchange labeling and two-dimensional NMR. *Annu. Rev. Biophys. Biomol. Str.* 21:243–265.

Jeng, M.-F., and S. W. Englander. 1991. Stable submolecular folding units in a non-compact form of cytochrome C. *J. Mol. Biol.* 221: 1045–1061.

Lafleur, L., J. Rice, and G. J. Thomas, Jr. 1972. Raman studies of nucleic acids VII. Poly(A)·poly(U) and poly(G)·poly(C). *Biopolymers.* 11: 2423–2437.

Lamba, O. P., R. Becka, and G. J. Thomas, Jr. 1990. Adenine and guanine 8CH exchange in nucleic acids: resolution and measurement by Raman optical multichannel analysis. *Biopolymers.* 29:1465–1477.

Li, T. 1992. Investigation of molecular recognition by static and dynamic

methods of Raman spectroscopy: applications to RNA plant viruses and DNA-protein complexes. Ph.D. thesis, School of Biological Sciences, University of Missouri-Kansas City.

Li, T., Z. Chen, J. E. Johnson, and G. J. Thomas, Jr. 1990. Structural studies of bean pod mottle virus, capsid and RNA in crystal and solution states by laser Raman spectroscopy. *Biochemistry*. 29:5018–5026.

Li, T., Z. Chen, J. E. Johnson, and G. J. Thomas, Jr. 1992. Conformations, interactions and thermostabilities of RNA and proteins in bean pod mottle virus: investigation of solution and crystal structures by laser Raman spectroscopy. *Biochemistry*. 31:6673–6682.

Lomonossoff, G. P., and J. E. Johnson. 1991. The synthesis and structure of comovirus capsids. *Prog. Biophys. Mol. Biol.* 55:107–137.

Lord, R. C., and G. J. Thomas, Jr. 1967. Raman spectral studies of nucleic acids and related molecules I. Ribonucleic acid derivatives. *Spectrochim. Acta*. 23A:2551–2591.

MacFarlane, S. A., M. Shanks, J. W. Davies, A. Zlotnick, and G. P. Lomonossoff. 1991. Analysis of the nucleotide sequence of bean pod mottle virus middle component RNA. *Virology*. 183:405–409.

Mandal, C., N. R. Kallenbach, and S. W. Englander. 1979. Base-pair opening and closing reactions in the double helix. *J. Mol. Biol.* 135:391–411.

Nakanishi, M., M. Tsuboi, Y. Saijo, and T. Nagamura. 1977. Stopped-flow ultraviolet spectroscopy for hydrogen exchange studies of nucleic acids. *FEBS Lett.* 81:61–64.

Preisler, R. S., C. Mandal, S. W. Englander, N. R. Kallenbach, F. B. Howard, J. Frazier, and H. T. Miles. 1981. Equilibrium and kinetic characteristics of the low temperature open state in polynucleotide duplexes. *In* Biomolecular Stereodynamics. R. H. Sarma, editor. Adenine Press, Guilderland, New York. 405–415.

Prescott, B., R. Gamache, J. Livramento, and G. J. Thomas, Jr. 1974. Raman studies of nucleic acids XII. Conformations of oligonucleotides and deuterated polynucleotides. *Biopolymers*. 13:1821–1845.

Rice, J., L. Lafleur, G. C. Medeiros, and G. J. Thomas, Jr. 1973. Raman studies of nucleic acids IX. A salt-induced structural transition in poly-(rG). *J. Raman Spectrosc.* 1:207–215.

Semancik, J. S., and J. B. Bancroft. 1965. Stability differences between the nucleoprotein components of bean pod mottle virus. *Virology*. 27:476–483.

Teitelbaum, H., and S. W. Englander. 1975. Open states in native poly-nucleotides. *J. Mol. Biol.* 92:55–92.

Thomas, G. J., Jr., and M. Tsuboi. 1993. Raman spectroscopy of nucleic acids and their complexes. *Adv. Biophys. Chem.* 3:1–70.